*computation*

MDPI

*Article*

# Advanced Control Scheme Optimization for Stand-Alone Photovoltaic Water Pumping Systems

**Maissa Farhat [1,2] and Oscar Barambones [2,*]**

[1] Department of Electrical & Electronics Engineering SOE, American University of Ras Al Khaimah, Building: 75, Seih Al Araibi, Ras Al Khaimah P.O. Box 10021, United Arab Emirates; maissa.farhat@aurak.ac.ae
[2] Advanced Control Group, Universidad del País Vasco (UPV/EHU), EI-VG, Nieves Cano 12, 01006 Vitoria, Spain
* Correspondence: oscar.barambones@ehu.eus

**Abstract:** This study introduces a novel method for controlling an autonomous photovoltaic pumping system by integrating a Maximum Power Point Tracking (MPPT) control scheme with variable structure Sliding Mode Control (SMC) alongside Perturb and Observe (P&O) algorithms. The stability of the proposed SMC method is rigorously analyzed using Lyapunov's theory. Through simulation-based comparisons, the efficacy of the SMC controller is demonstrated against traditional P&O methods. Additionally, the SMC-based system is experimentally implemented in real time using dSPACE DSP1104, showcasing its robustness in the presence of internal and external disturbances. Robustness tests reveal that the SMC controller effectively tracks Maximum Power Points (MMPs) despite significant variations in load and solar irradiation, maintaining optimal performance even under challenging conditions. The results indicate that the SMC system can achieve up to a 70% increase in water flow rates compared with systems without MPPT controllers. Furthermore, SMC demonstrated high sensitivity to sudden changes in environmental conditions, ensuring efficient power extraction from the photovoltaic panels. This study highlights the advantages of integrating SMC into Photovoltaic Water Pumping Systems (PV-WPSs), providing enhanced control capabilities and optimizing system performance. The findings contribute to the development of sustainable water supply solutions, particularly in remote areas with limited access to the electrical grid.

**Keywords:** photovoltaic; MPPT; sliding mode control; dSPACE; DC motor; pump; boost



**Citation:** Farhat, M.; Barambones, O. Advanced Control Scheme Optimization for Stand-Alone Photovoltaic Water Pumping Systems. *Computation* **2024**, *12*, 224. https://doi.org/10.3390/computation12110224

Academic Editor: Demos T. Tsahalis

Received: 25 September 2024
Revised: 31 October 2024
Accepted: 7 November 2024
Published: 11 November 2024



## 1. Introduction

Renewable energy sources have gained significant attention in recent years, driven by the urgent need to reduce greenhouse gas emissions and mitigate climate change. Among the promising solutions is the integration of photovoltaic (PV) technology into transportation infrastructure, particularly through photovoltaic carports [1–3]. This innovative application serves a dual purpose: generating clean electricity while providing valuable shading for parked vehicles. The adoption of PV technology is also rising in residential and commercial settings, with the industry increasingly exploring more creative applications, such as building-integrated photovoltaic systems, as society continues to seek ways to harness and integrate renewable energy.

In addition to these applications, the significance of an efficient irrigation system in remote areas is closely tied to the accessibility of electricity. Unfortunately, many regions in the developing world suffer from inadequate access to electricity grids. However, the advancement of photovoltaic technology, which captures solar energy and converts it into electrical power, presents a promising solution for water pumping systems in sunny areas. Photovoltaic-driven water pumping systems, also known as Photovoltaic Water Pumping Systems (PV-WPSs), are among the most prevalent applications of solar energy in developing countries, significantly contributing to economic and social development. For remote areas, a PV-WPS is the best option for bringing water.

One effective way to enhance the efficiency of these systems is through the use of solar trackers. Solar trackers dynamically adjust the orientation of PV panels to follow the sun's path, significantly increasing energy capture throughout the day. This capability can lead to improved performance in irrigation systems, making them more effective in delivering water to crops in areas where every drop counts.

The authors in [4] present a design for a solar tracker specifically tailored for irrigation systems. The paper details the mechanical and electronic components used, demonstrating how the tracker can significantly enhance the performance of solar-powered water pumps, leading to improved crop yields. The authors in article [5] discuss the cost–benefit analysis of implementing solar trackers for water pumping. The findings suggest that, while initial investment is higher for tracking systems, the long-term savings on energy costs and the increased water output make them economically viable for farmers. The research in [6] investigates the impact of solar tracking on the overall efficiency of water pumping systems. The results indicate that solar trackers not only improve the energy output but also reduce the operational costs associated with water pumping in remote areas. The investigation in [7] explores the integration of solar trackers with smart water management technologies. The authors highlight how real-time data from solar trackers can optimize water usage in agricultural practices, ensuring that pumps operate only when necessary, thereby conserving energy. The study in [8] evaluates the efficiency of single-axis and dual-axis solar tracking systems in powering water pumps. The authors found that dual-axis trackers increased energy capture by up to 40% compared with fixed systems, resulting in more reliable water pumping, especially in regions with variable sunlight. Solar trackers are systems that optimize solar energy production by adjusting the angle of solar panels throughout the day to follow the sun's path. The primary advantage of solar trackers is their ability to increase energy output by 20% to 50% compared with fixed installations, resulting in improved efficiency and a higher return on investment. However, they come with higher initial costs and more complex maintenance requirements due to their moving parts. Additionally, while they can maximize energy capture in limited spaces, trackers may require more land and can be vulnerable to damage from severe weather conditions. Overall, the decision to use solar trackers involves weighing their benefits against the associated costs and maintenance challenges. In addition, a PV pumping system is usually not equipped with batteries for storage purposes due to the fact that water can be filled into tanks that can be used at night time during the unavailability of light. An alternative to solar trackers is the use of Maximum Power Point Tracking (MPPT) algorithms. MPPT technology continuously adjusts the electrical load to ensure that the solar panels operate at their maximum power output, regardless of varying sunlight conditions. This approach offers the advantage of requiring fewer moving components, resulting in lower maintenance needs compared with solar trackers.

The goal of this work is to maximize the effectiveness and the water output pumped by the stand-alone PV pumping system by using the MPPT control. It is crucial to understand that the PV power generated is affected by weather conditions [9]. A PV system's success is therefore determined by a number of factors (irradiation, temperature, etc.). Under stable conditions, the Power versus Voltage (P-V) curve displays a single Maximum Power Point (MPP) [2], where the PV system achieves the highest possible electrical power output. The typical operating condition of a PV system coupled directly to a load is often not at the MPP. Therefore, to achieve a high power rate from a PV system, power electronics converters are indispensable. Hence, the reliability of the MPPT controller is critical for the effective and productive operation of the PV system [10,11]. However, implementing MPPT control presents significant difficulties, primarily because the Photovoltaic Generator (PVG) is affected by constant external disturbances due to fluctuating sunlight conditions.

Several methods have been developed for the MPPT in PV systems [12], each offering unique advantages and facing specific challenges. Traditional algorithms such as the Perturb and Observe (P&O), Incremental Conductance (INC) [13], and Fractional Open Circuit and Short Circuit algorithms are favored for their straightforward implementation

and affordability [14]. These methods adjust the PVG's operating point based on a fixed step size, which may limit accuracy under changing conditions [15].

Unconventional techniques like Artificial Neural Networks (ANNs) and Fuzzy Logic Controllers (FLCs) offer higher complexity but improved performance in specific conditions [16]. The FLC, known for its robustness and immunity to disturbances, has been applied successfully in various fields, including photovoltaic systems [17]. However, the FLC's reliance on a large and complex rule base can lead to scalability challenges and increased computational demands [18].

Artificial Neural Networks (ANNs), while capable of strong performance, have drawbacks such as requiring prior knowledge of system behaviors and large datasets for effective learning [19]. Rapid changes in weather conditions can also impact the performance of ANNs due to their reliance on historical data and learning processes [20].

Nonlinear controllers, such as Sliding Mode Control (SMC), are gaining attention due to their robustness and effectiveness in dynamic environments [21]. In the Sliding Mode Control (SMC) framework, a trajectory is set for the objective function, and the control structure is modified according to the system's state to reach the control objectives [22], thereby mitigating external disturbances and internal parameter variations [22]. Research indicates that SMC offers superior performance in motor speed control compared with FLCs and classical Proportional–Integral–Derivative (PID) controllers [23]. Given the proven performance of SMC in various applications, including robotics, motor control, and power electronics [24–26], we have selected it for our photovoltaic pumping system. SMC's ability to maintain optimal performance despite varying environmental conditions makes it well suited for maximizing power output and ensuring the reliability of our PV pumping system [27]. This choice underscores our commitment to implementing a robust and effective MPPT strategy tailored to the specific demands of photovoltaic applications.

In this paper, we delve into the application of the variable structure Sliding Mode Control (SMC) in Photovoltaic Water Pumping Systems (PV-WPSs) and investigate the efficacy of SMC in achieving superior water flow rates compared with traditional techniques through simulation studies comparing SMC with the P&O algorithm using a motor pump as load and through real-time experiments utilizing a resistive load. The aim of this work is to demonstrate how Sliding Mode Control (SMC) can optimize the performance and enhance the efficiency of PV-WPSs, ultimately contributing to the advancement of sustainable water supply solutions.

Solar PV water pumping systems offer reliability and cost-effectiveness, making them a viable alternative to manual pumps, especially when deployed in suitable locations. Unlike traditional systems, solar-powered water pumping systems do not necessitate the use of batteries for power storage if water can be stored in tanks for nighttime use. In basic solar-powered water pumping systems, the solar panels are directly linked to a small DC motor that powers the water pump. These setups typically utilize a centrifugal pump due to its compatibility with solar panel output [28]. However, displacement pumps have distinct speed–torque characteristics and are not ideally suited for direct connection to solar panels. In such cases, power conditioning or MPPT is often incorporated between the PVG and the motor-pump to optimize energy conversion. Various types of motors are employed in water pumping systems, each with distinct benefits and drawbacks that determine the suitability for specific applications. When AC motors are utilized, an inverter is required between the PV panel and the motor, which adds to the overall system cost compared with DC motor-based water pumps [29,30]. Furthermore, DC motors offer additional advantages over other motor types, including higher starting torque, rapid starting and stopping capabilities, reversible rotation, and variable speed control through voltage input. Additionally, DC motors provide high-quality performance and durability, making them a preferred choice for various water pumping applications [31].

This study compares the effectiveness of the variable structure Sliding Mode Control (SMC) and Perturb and Observe (P&O) algorithms in achieving the Maximum Power Point Tracking (MPPT) in stand-alone PV pumping systems. While SMC offers robustness against

parameter uncertainties and disturbances through its nonlinear control strategy, P&O is renowned for its straightforward nature and ease of implementation. By conducting simulation-based comparisons, this study evaluates the performance of both methods under varying environmental conditions and load profiles. The results highlight the superior tracking accuracy and efficiency of the SMC-based MPPT controller compared with P&O, particularly in scenarios involving rapid irradiance changes or partial shading. Furthermore, experimental results using dSPACE DSP1104s demonstrate the practical viability of the SMC approach and showcase its ability to maintain stable and efficient operation against internal and external disturbances

This paper is organized as follows: Section 2 describes the configuration of an autonomous photovoltaic pumping system, detailing key components and the mathematical models governing their interactions. Section 3 discusses various Maximum Power Point Tracking (MPPT) control algorithms, including Perturb and Observe (P&O), Incremental Conductance (INC), and Sliding Mode Control (SMC), comparing their complexities and efficiencies while highlighting SMC's robustness in dynamic environments through a stability study. Section 4 presents results demonstrating that the SMC MPPT algorithm significantly outperforms the P&O algorithm, achieving up to 70% higher water flow rates under varying conditions. Finally, Section 5 concludes the paper, summarizing key contributions and suggesting future research directions.

## 2. Energy Conversion Stage

This section provides a detailed overview of the configuration of an autonomous photovoltaic pumping system. It describes the essential components, including the Photovoltaic Generator (PVG) and the DC converter and motor-pump, while also introducing the mathematical models that govern their operation and interactions. The importance of energy conversion is underscored, as it plays a crucial role in optimizing the system's overall performance for efficient water pumping. Figure 1 illustrates the main components, highlighting the PVG, which converts solar energy into electricity; the DC converter, which adjusts the output voltage from the PV arrays; and the digital controller, which employs Maximum Power Point Tracking (MPPT) algorithms to enhance system efficiency. Finally, the section discusses the DC motor-pump, which is integral to the water pumping process.

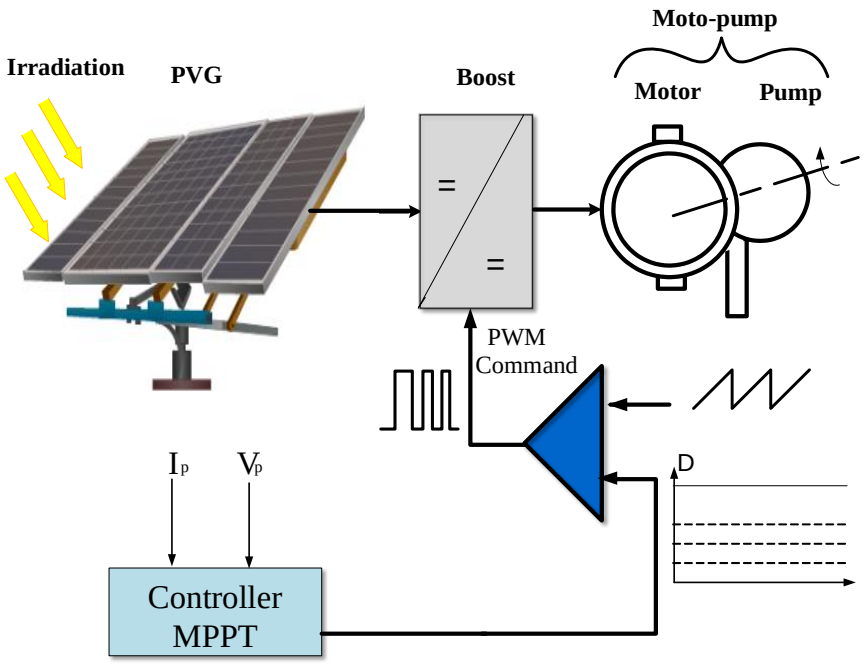


**Figure 1.** The proposed PV pumping system diagram.

In the modeling process of PV systems, significant attention is directed towards both the motor-pump (as a load) and the energy conversion stage. This stage primarily consists of the PV panel and the DC converter, which play crucial roles in matching the output of the PV panels to the load.

### *2.1. PVG Model*

The primary function of the PV panel is to convert sunlight into electrical energy through the photovoltaic effect. Composed of interconnected solar cells, the panel generates Direct Current (DC) electricity upon exposure to sunlight. Its equivalent electric circuits containing a diode, a resistance, and a power supply can be substituted for a PV cell.

Figure 2 illustrates a simplified equivalent circuit of a photovoltaic (PV) cell, depicting its key components, including the current source, diode, and resistances. This representation is crucial for understanding the operational principles of a PV cell, as it highlights how the photovoltaic effect generates electrical energy from solar radiation.

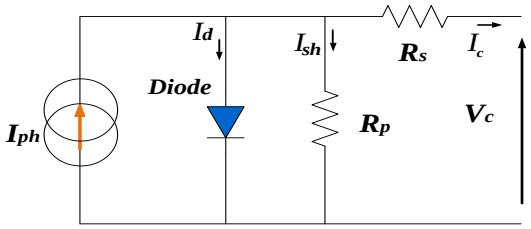


**Figure 2.** PV cell equivalent circuit.

Depending on the received temperature and irradiation, the power supply produces an $I_{ph}$ current [12,32,33]. Utilizing Kirchhoff's Current Law (KCL)

$$I_c = I_{ph} - I_{diode} - I_{sh} \tag{1}$$

The $I_{ph}$ can be written as: [12]

$$I_{ph} = \frac{G}{G_{ref}}\left(I_{rs\_ref} + K_{SCT}\left(T_c - T_{ref}\right)\right) \tag{2}$$

$$I_d = I_{sc}\left(exp\frac{q(V_c + R_s I_c)}{\alpha\beta T} - 1\right) \tag{3}$$

$$I_{sh} = \frac{1}{R_p}(V_c + R_s I_c) \tag{4}$$

One can obtain an approximate value for the reverse saturation current [12]:

$$I_{sc} = \frac{I_{sc\_ref}}{exp\left[\frac{qV_{oc}}{n_s.\alpha.\beta.T_c}\right] - 1} \tag{5}$$

The expression for the cell current $I_c$ is

$$I_c = I_{ph} - I_{sc}\left(exp\frac{q(V_c + R_s I_c)}{\alpha kT} - 1\right) - \frac{1}{R_p}(V_c + R_s I_c) \tag{6}$$

The PVG relies on the configuration of cells, specifically the number in series ($N_s$) and in parallel ($N_p$).

$$\begin{cases} I_p = N_p I_c \\ V_p = N_s n_s V_c \end{cases} \tag{7}$$

To conclude, we can provide the PVG current ($I_p$) by

$$I_p = N_p I_{ph} - N_p I_{sc}\left(exp\frac{q}{\alpha kT}\left(\frac{V_p}{n_s N_s} + \frac{R_s I_P}{N_p}\right) - 1\right) - \frac{N_p}{R_p}\left(\frac{V_p}{n_s N_s} + \frac{R_s I_P}{N_p}\right) \quad (8)$$

assuming $R_p > R_s$ allows the elimination of terms involving $R_s$ and $R_p$, the ideal case assumes $R_s = 0$ and $R_p = \infty$ [12].

$$I_p = N_p I_{ph} - N_p I_{sc}\left(exp\frac{q}{n\beta T_c}\left(\frac{V_p}{n_s N_s}\right) - 1\right) \quad (9)$$

The commercial PV module A55 manufactured by ATERSA has been chosen in this work. There are thirty-six monocrystalline cells, all connected in series ($n_s$ = 36) in this module. Table 1 shows the manufacturing specifications.

**Table 1.** ATERSA specifications.

| Cell Type | Monocrystalline | Unit |
|---|---|---|
| $P_{mpp}$ | 55 | [W] |
| *Voc* | 20.5 | [V] |
| *Isc_ref* | 3.7 | [A] |
| *Vmpp* | 16.2 | [V] |
| *Impp* | 3.4 | [A] |
| *ns* | 36 | - |

With dimensions of 637 × 527 × 35, the ATERSA A55 module is not only effective for small systems but also scalable to large installations. The performance of a solar cell is evaluated under a Standard Test Condition (STC). For this scenario, the irradiance is set to 1000 W/m$^2$, and the temperature is kept at 25 °C.

### *2.2. Boost Converter*

The topologies of the DC converter are designed to satisfy specific DC load requirements. In this case, the converter can function as a switching mode controller by increasing or decreasing the DC output voltage by using power switching devices to perform at a fixed frequency. The DC boost converter was selected for the simulation and real-time experimental validation in this study.

Figure 3 illustrates the basic circuit topology of a boost converter, which contains a switch ($S_w$), a diode, an inductor (L), a capacitor (C2), a switching controller, and a load (Rout) characterized by a voltage (Vout), and additional capacitor (C1) is added at the input level to stabilize the input voltage (Vin) signal. It is possible to use this topology as an interface between a PVG and a battery bank or between a PVG and any DC load. In this work, the load is the motor-pump [34–36].

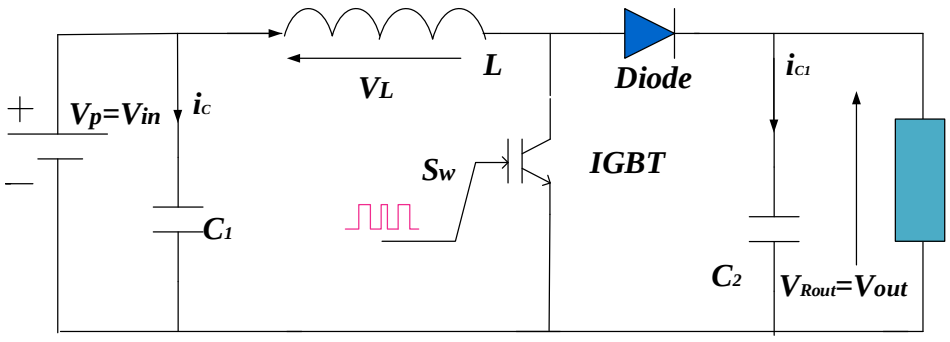


**Figure 3.** Converter circuit.

Under Continuous Conduction Mode (CCM), the relationship between the converter's output voltage and its input voltage is given by:

$$V_{out} = \frac{1}{1-D} V_{in} \tag{10}$$

$D$ represents the duty cycle.

Assuming that $P_{in} = P_{out}$ and that the power formula can be rewritten using Ohm's law as $P = V^2/R$, the following can be deduced:

$$R_{out} = \frac{1}{(1-D)^2} R_{pv} \tag{11}$$

where $R_{pv}$ represents the load seen by the PVG through the boost converter, $R_{out}$ is the load seen by the boost converter, $S_w$ is the switch state command, $S_w = 0$ indicates that the switch is off, and $S_w = 1$ indicates that the switch is on.

According to the boost converter model, the Equation (11) relationship is given by: $R_{pv} = (1-D)^2 \cdot R_{out}$. This equation shows that if the duty cycle $D$ decreases, $R_{pv}$ increases; and if $D$ increases, $R_{pv}$ decreases. This relationship can be understood in the context of the PV module's dynamic behavior, as illustrated by the Current versus Voltage (I-V) characteristic in Figure 4, when $I_p$ decreases/increases and $V_p$ increases/decreases. Accordingly, duty cycle changes always oppose voltage changes. Mathematically, this can be expressed as follows:

$$sign(\dot{V}_{in}) = -sign(\dot{D}) \tag{12}$$

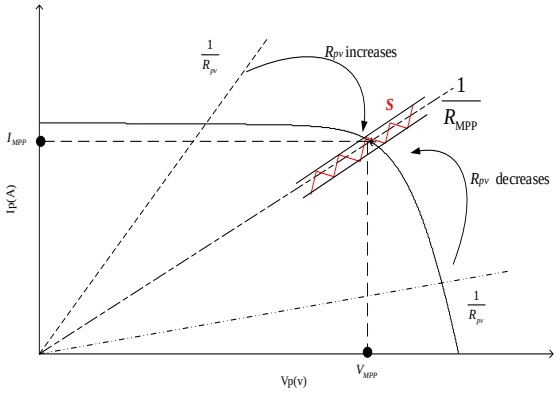


**Figure 4.** I-V characteristics.

The boost converter specifications for this project are shown below in Table 2.

**Table 2.** Boost specifications.

| Component | Characteristic | |
|---|---|---|
| Schottky Diode | 2× MURF1560GT | 600 V, 15 A, 0.4 V at 10 A, 150 °C |
| IGBT | 1× HGT40N60B3 | 600 V, 40 A, 1.5 V at 150 °C |
| L | 6× PCV-2-564-08 | 560 µH, 7 A, 42 mΩ |
| C1, C2 | 2× TK Series | 1500 µF, 250 V |

The boost converter circuit dynamic model is obtained by applying Kirchhoff's Current Law (KCL) and Kirchhoff's Voltage Law (KVL):

$$\begin{cases} \frac{dV_p}{dt} = \frac{1}{C_1}(i_p - i_L) \\ \frac{di_L}{dt} = \frac{1}{L}V_p + \frac{1}{L}(S_W - 1)V_{out} \\ \frac{dV_{out}}{dt} = \frac{1}{C_2}(i_L - i_{out}) - \frac{1}{C_2}S_W i_L \end{cases} \tag{13}$$

$$\dot{x} = f(x) + g(x)S_W \tag{14}$$

where

$$x = \begin{bmatrix} V_p \\ i_L \\ V_{out} \end{bmatrix},$$
$$f(x) = \begin{bmatrix} \frac{1}{C_1}(i_p - i_L) \\ \frac{1}{L}(V_p - V_{out}) \\ \frac{1}{C_2}(i_L - i_{out}) \end{bmatrix}, \tag{15}$$
$$g(x) = \begin{bmatrix} 0 \\ \frac{1}{L}V_{out} \\ -\frac{1}{C_2}i_L \end{bmatrix},$$

### *2.3. Motor-Pump*

There are a variety of pumping systems available [37]. In the case of submersible pumps, they remain below the surface of the water, whereas surface pumps are mounted at water level, and floating pumps are mounted above the surface of the water. Pumps are categorized depending on their operating mode. Positive displacement pumps and centrifugal ones are commonly used types of pumps. When compared with centrifugal pumps, positive displacement pumps are more efficient at low power levels [37].

The DC motor-pump model can be given as: [38,39].

$$\begin{cases} L_a \frac{di_a}{dt} = U_a - R_a i_a - K_t \omega \\ j \frac{d\omega}{dt} = T_{em} - T_l - f\ \omega \end{cases} \tag{16}$$

Water flow in positive displacement pumps is a function of the shaft speed. The load torque for such a pump is given by the following equation [40].

$$T_L = T_1 \cdot \omega + T_2 \tag{17}$$

where $T_1$ and $T_2$ are the torque constant. The mathematical model proposed connects the water flow rate in the pump to the power $P$ and the water column height $h$ [41]. The $e_i$, $f_i$, $m_i$, $n_i$, and $d_i$ are secondary parameters dependent on the pump's type.

$$P(Q,h) = s(h)Q^3 + z(h)Q^2 + m(h)Q + n(h) \tag{18}$$

$$\begin{cases} s(h) = s_0 + s_1 h^1 + s_2 h^2 + s_3 h^3 \\ z(h) = z_0 + z_1 h^1 + z_2 h^2 + z_3 h^3 \\ m(h) = m_0 + m_1 h^1 + m_2 h^2 + m_3 h^3 \\ n(h) = n_0 + n_1 h^1 + n_2 h^2 + n_3 h^3 \end{cases} \tag{19}$$

An example of a DC motor-pump available on the market is the Grundfos CMBE PM1, which is designed for water supply and irrigation systems. This pump uses a DC motor with integrated variable speed control to adjust the flow rate based on demand, ensuring efficient energy consumption.

The selected pump model, Grundfos CMBE PM1, is a DC motor positive displacement pump commonly used for water supply and irrigation. It features a variable speed control system, ensuring optimal performance and energy efficiency. The mathematical model of this pump aligns with the torque and water flow equations presented, where the water flow rate is directly related to the shaft speed. The pump's parameters, such as torque constants and power relationships to water column height, are detailed and consistent with Equations (16)–(18) described in the study.

## 3. MPPT Control Algorithms

The objective of this section is to explore various Maximum Power Point Tracking (MPPT) control algorithms that are essential for enhancing the performance of photovoltaic

systems and to discuss techniques such as Perturb and Observe (P&O), Incremental Conductance (INC), and Sliding Mode Control (SMC), comparing their complexities, efficiencies, and capabilities in handling transient responses. The section emphasizes that, while simpler methods like P&O are effective under stable conditions, advanced approaches like SMC offer superior performance in dynamic environments.

MPPT techniques are essential for optimizing the performance of PV systems. These methods vary in complexity, implementation requirements, and performance under different conditions. MPPT algorithms include common approaches like Perturb and Observe or Incremental Conductance as well as advanced approaches like Fractional Open Circuit and Short Circuit methods. Each technique has its strengths and limitations, which are crucial for selecting the most suitable method based on the specific needs of the PV system. The following Table 3 provides a comparative overview of several MPPT controllers, highlighting their complexity, implementation, accuracy, data requirements, convergence time, and the absolute value of their over or undershooting [12–27]. The over and undershoot phenomenon refers to the system's transient response when there is a sudden change in input, such as variations in irradiance or load demand. In control systems, overshoot occurs when the system output temporarily exceeds its desired value before stabilizing, while undershoot happens when the output falls below the desired value. These behaviors are critical for evaluating the system's stability and performance.

**Table 3.** Comparative overview MPPT controllers.

| Controller | Complicity/Price | Implementation | Accuracy | Requires Datasets | Convergence Time | Over/or Undershoot |
|---|---|---|---|---|---|---|
| P&O | Low cost, low complexity. Simple to implement with low hardware requirements but limited in dynamic conditions. | Easy | Low; may not perform well under rapidly changing conditions. | No | 0.4 s [12] | 0.18 [12] |
| Incremental Conductance | Moderate cost, moderate complexity. Requires additional sensors and tuning but offers better control accuracy. | Easy but more complex than P&O; requires more computational resources. | Low; may exhibit reduced performance in conditions with rapid changes. | No | 0.6 s [12] | 0.050179 [12] |
| Fractional Open Circuit and Short Circuit | Low cost, low complexity. Simple to implement but less accurate under varying irradiance conditions. | Easy | Low; may exhibit reduced performance in conditions with rapid changes. | No | 0.7 s [12] | 0.03405 And 0.030466 [12] |
| Fuzzy Logic Controllers | High cost, moderate to high complexity. Needs sophisticated tuning and rule-based algorithms. | Design can be complex; requires expert knowledge to set membership functions. | High | Yes | 0.3 s [12] | 0.73 [12] |
| ANNs | High cost, high complexity. Requires advanced processors, data training, and significant tuning. | Requires large datasets for training; complex model design. | High | Yes | 0.75 s MSE = 1.4793 $\times 10^{-9}$ [19] | 0.11 [19] |
| SMC in this work | Moderate to high cost, high complexity. Requires more implementation effort but delivers optimal performance. | Easy | High | No | 0.1 s | 0.038462 |

In the context of our Photovoltaic Water Pumping System (PV-WPS), the controllers exhibit different levels of overshoot and undershoot depending on their ability to handle

sudden changes. For instance, the P&O controller tends to have more significant overshoot due to its slower dynamic response, while the Sliding Mode Control (SMC) minimizes both over and undershoot due to its robustness and quick response to disturbances.

The performance of various Maximum Power Point Tracking (MPPT) controllers—Perturb and Observe (P&O), Incremental Conductance (INC), Fractional Open Circuit Voltage (FOCV), Fuzzy Logic Controller (FLC), Artificial Neural Networks (ANNs), and Sliding Mode Control (SMC)—varies significantly in terms of daily power output, energy efficiency, and pumped water volume. The P&O method, while effective under stable conditions, often exhibits oscillations around the Maximum Power Point (MPP) during rapid changes in irradiance, resulting in moderate daily energy output [42] In contrast, the INC controller demonstrates superior responsiveness to changing conditions, typically yielding higher energy outputs than P&O [43]. The FOCV method, characterized by its simplicity, may not track the MPP as effectively in dynamic environments, leading to lower energy production compared with INC and P&O. Fuzzy Logic Controllers (FLCs) offer adaptability in uncertain conditions, often achieving competitive energy outputs [44]. ANN-based controllers can potentially maximize daily energy output, contingent on the quality of training data, while SMC provides robust performance across varying conditions, consistently delivering high energy output. Consequently, systems employing SMC are likely to pump more water daily due to their enhanced efficiency in dynamic scenarios. Table 4 includes a summary table detailing the advantages, disadvantages, and efficiency results of each method assessed.

**Table 4.** Summary of MPPT performance assessment methods.

| Method | Advantages | Disadvantages | Efficiency Results |
|---|---|---|---|
| P&O | Simple, low resource use | Oscillates in dynamic conditions | 90% [42] |
| INC | High responsiveness | More complex, higher resource use | 95% [43] |
| FOCV | Simple, fewer measurements | Less effective in rapid changes | 85% [44] |
| FLC | Robust, adaptable | Complex tuning required | 92% [45] |
| ANNs | Handles nonlinearities | Requires extensive training data | 94% [46] |
| SMC | Consistent performance | Complex implementation | 96% [47] |

Sliding Mode Control (SMC) is a robust control technique that has garnered significant attention in recent years [48–51]. One of the key advantages of SMC is its ability to handle system uncertainties and disturbances [48,51].

Recent research papers have extensively explored Sliding Mode Control (SMC) strategies in various applications. Laware's study compared SMC and PID control for DC motor applications, concluding that SMC outperforms PID controllers in speed control [52]. Tverskoi delved into Discrete Time Sliding Mode Control (DTSMC) for third-order processes, emphasizing stability and system response improvement [53]. Another paper compared backstepping, sliding mode, and PI controls for active power filters, favoring backstepping for harmonic minimization and reactive power compensation [54]. Sakri et al. focused on SMC for three-phase pulse-width modulation rectifiers, achieving stability and dynamic performance enhancements through sliding mode strategies [55]. Ruderman et al. investigated continuous higher order sliding mode (CHOSM) controllers for disturbance rejection, highlighting the effectiveness of CHOSM, particularly in comparison with PID controllers, for broadband disturbance rejection [56]. These studies collectively showcase the versatility and effectiveness of SMC techniques in diverse control engineering applications.

One of the key advantages of Sliding Mode Control (SMC) is its ability to handle system uncertainties and disturbances [48,51] Compared with other control methods, SMC offers a unique approach known as variable structure control, which has been the subject of extensive research [50,57]. The variable structure control aspect of SMC is particularly

important as it allows the control system to adapt its structure dynamically based on the system's current state [50,57]. This adaptability is achieved through the use of a sliding surface, which defines the desired system behavior [48,51]. By maintaining the system's state on the sliding surface, the variable structure control can effectively compensate for uncertainties and disturbances, leading to a highly robust and reliable control system [48,50]. In contrast to other SMC methods, the variable structure control approach offers several advantages [50,57], as it is capable of providing desirable full-order system dynamics during the sliding mode rather than reduced-order dynamics [50]. Additionally, the variable structure control can be designed to be chattering-free, which is a common issue in traditional SMC [50,57].

Overall, the significance of the variable structure control aspect of Sliding Mode Control (SMC) lies in its ability to adapt the control system's structure dynamically, leading to enhanced robustness, reliability, and performance [48,50,51,57].

In this paper, we compared the behavior of the variable structure Sliding Mode Control (SMC) with the Perturb and Observe (P&O) algorithm.

Knowing that the PV power is $P = V_p I_p$, we can find the MPP of the PVG through finding a solution for the following function. The graph in Figure 5 illustrates the variation in power with respect to voltage for the photovoltaic (PV) system, highlighting the relationship between these two critical parameters. As the voltage increases, the power output of the PV system initially rises, reaching a peak at the Maximum Power Point (MPP) before subsequently declining

$$\frac{\partial P}{\partial V_p} = 0 \tag{20}$$

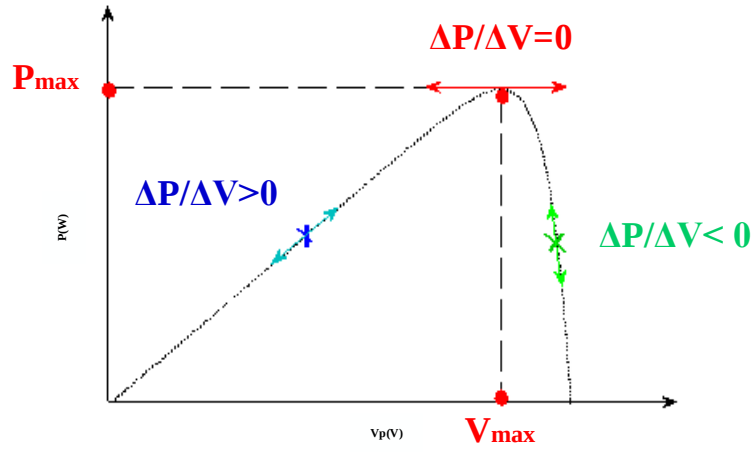


**Figure 5.** Variation in power with respect to voltage.

So

$$\frac{\partial P}{\partial V_p} = I_p + \frac{\partial Ip}{\partial V_p} V_p \tag{21}$$

### *3.1. Perturb and Observe*

This algorithm stands out as the most popular MPPT method due to its simplicity and effectiveness [58–61]. The PV module power is varied by introducing a minor perturbation. Power output from PV systems is measured at intervals and compared with past values in the P&O algorithm. If the output power increases, the procedure is continued; if it decreases, the perturbation is reversed. Figure 6 presents the flowchart of the Perturb and Observe (P&O) algorithm, outlining the systematic process used for Maximum Power Point Tracking (MPPT) in photovoltaic systems. The flowchart visually represents the steps involved in the P&O method.

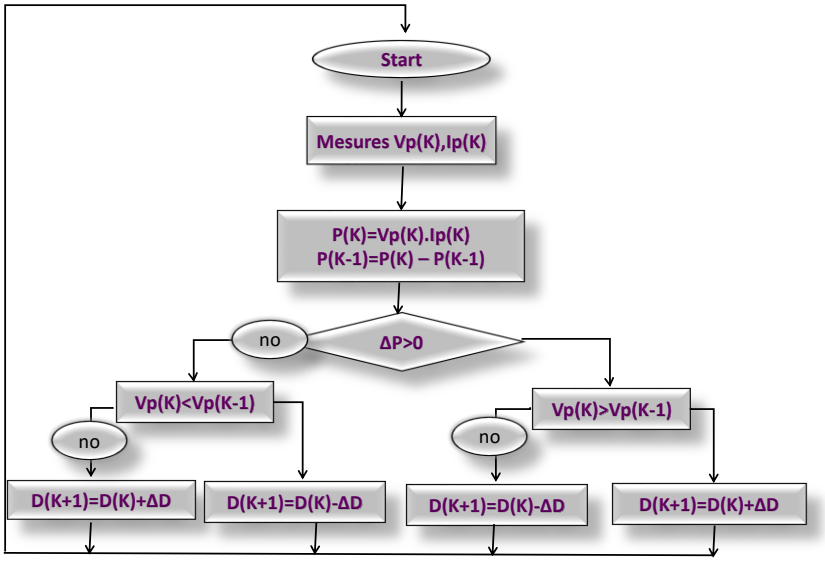


**Figure 6.** The P&O algorithm flowchart.

The step size increment $\Delta D$ in the P&O algorithm is determined through a trial-and-error process, where selecting a step size that is either too large or too small can lead to instability. Although the P&O algorithm is simple to implement, it suffers from several issues, including the inability to consistently track the MPP and oscillatory behavior in PV systems. While larger perturbations can result in faster convergence to the MPP, they also increase power losses, whereas smaller $\Delta D$ values reduce power loss but slow down the tracking speed. Therefore, selecting the optimal $\Delta D$ is a significant challenge [61,62]. To address these issues, this work proposes the use of Sliding Mode Control (SMC) with a variable structure mode as an advanced MPPT method to improve tracking performance and system efficiency.

### *3.2. Variable Structure Sliding Mode Algorithm*

To track Maximum Power Points (MMPs), variable structure control systems based on sliding mode algorithms are used, which consist of a set of laws for feedback control and a set of rules for decision making. Based on the behavior of the systems, in this case the PV panel output power, the switching function determines which feedback control to apply.

$S = 0$ is the switching surface. Two parts of the state space exist, $S < 0$ and $S > 0$ [63]

The algorithm switching function is given by

$$S = \frac{\partial P}{\partial V_p} = I_p + \frac{\partial ip}{\partial V_p} V_p \tag{22}$$

Figure 5 illustrates two distinct states of the PVG. The control function for the converter's power gate drive signal is determined by

$$S_W \begin{cases} 1 & S < 0 \\ 0 & S > 0 \end{cases} \tag{23}$$

Let

$$\dot{S} = \frac{\partial S}{\partial x^T} \dot{x} = \frac{\partial S}{\partial x^T} f(x) + \frac{\partial S}{\partial x^T} g(x) S_{W_{eq}} = 0 \tag{24}$$

**Proof.** According to [64], demonstrating the effectiveness of the variable structure mode control involves showing that the Lyapunov function meets the following conditions:

$$\begin{array}{c} V = \frac{1}{2}S^2 > 0, \\ \dot{V} = S\frac{dS}{dt}, \\ S\dot{S} < 0 \end{array} \tag{25}$$

By using Equation (23), the system can be stabilized from any initial state, demonstrating the effectiveness of this approach.

$$\begin{cases} S = \frac{\partial P}{\partial V_p} = I_p + \frac{\partial Ip}{\partial V_p}V_p \\ \text{with } \; I_p = N_p I_{ph} - N_p I_{rs}\left(exp\frac{q}{n\beta T_c}\left(\frac{V_p}{n_s N_s}\right) - 1\right) \end{cases} \tag{26}$$

$$\begin{array}{l} S = \frac{\partial P}{\partial V_p} = I_p + \frac{\partial Ip}{\partial V_p}V_p \\ = N_p I_{ph} - N_p I_{rs}\big(exp\big(AV_p\big) - 1\big) - N_p I_{rs} A exp\big(AV_p\big)V_p \end{array} \tag{27}$$

with $A = \frac{q}{n\beta T_c}\frac{1}{n_s N_s}$.

***Case 1: S > 0***

According to Figure 5, if the system operates on the left side where $S_W = 0$, the switch is off, which leads to a decrease in the duty cycle. Consequently, this decrease in the duty cycle causes the voltage $V_p$ to increase.

$$\frac{dV_p}{dt} > 0 \tag{28}$$

$$\frac{dS}{dt} = N_p\Big[\Big(I_{ph} - I_{rs}\Big) - I_{rs}\big(1 + AV_p\big)exp\big(AV_p\big)\Big]' \tag{29}$$

$$\frac{dS}{dt} = -N_p I_{rs} A\big[exp\big(AV_p\big) + \big(1 + AV_p\big)exp\big(AV_p\big)\big]\dot{V}_p \tag{30}$$

Using Equation (28) in Equation (30) gives: $\frac{dS}{dt} < 0$.

Finally, $S\frac{dS}{dt} < 0$.

***Case 2: S < 0***

If the system is operating on the right side with $S_W = 1$, the switch command is high, resulting in an increase in the duty cycle and a subsequent decrease in $V_p$

$$\frac{dV_p}{dt} < 0 \tag{31}$$

So, $\frac{dS}{dt} > 0$ and $S\frac{dS}{dt} < 0$.

Ultimately, the system attains a globally stable condition through the application of the proposed methods. □

## 4. Results

This section presents and analyzes the results of the implemented Maximum Power Point Tracking (MPPT) control algorithms for the autonomous photovoltaic pumping system. This section is divided into two parts: simulation results and experimental results. It aims to demonstrate the effectiveness of the proposed Sliding Mode Control (SMC) algorithm compared with the Perturb and Observe (P&O) algorithm in terms of performance metrics such as water flow rates, response time, and robustness under varying irradiance and load conditions. By showcasing these results, the section highlights the advantages of SMC in maximizing power extraction and improving the overall efficiency of the photovoltaic system.

### *4.1. Simulation Result*

This section focuses on the implementation of the global control strategy for the solar-powered water pumping system discussed in Section 2 and depicted in Figure 1. The proposed MPPT algorithm adjusts the converter's duty cycle to maintain optimal load voltage and enhance water pumping efficiency. The algorithm also highlights the significance of each figure in relation to the findings.

Figure 7 presents the results of simulations conducted at irradiation levels of 1000 W/m$^2$ and 500 W/m$^2$, along with abrupt changes in irradiance (G). This figure effectively illustrates the dynamic response of the MPPT algorithm, including the generated duty cycle (D), motor speed ($\omega$), and armature current ($i_a$). The graphical representation allows for a clear comparison of how the MPPT algorithms respond to varying conditions, emphasizing the robustness of the Sliding Mode Control (SMC) in adapting to sudden changes in irradiance.

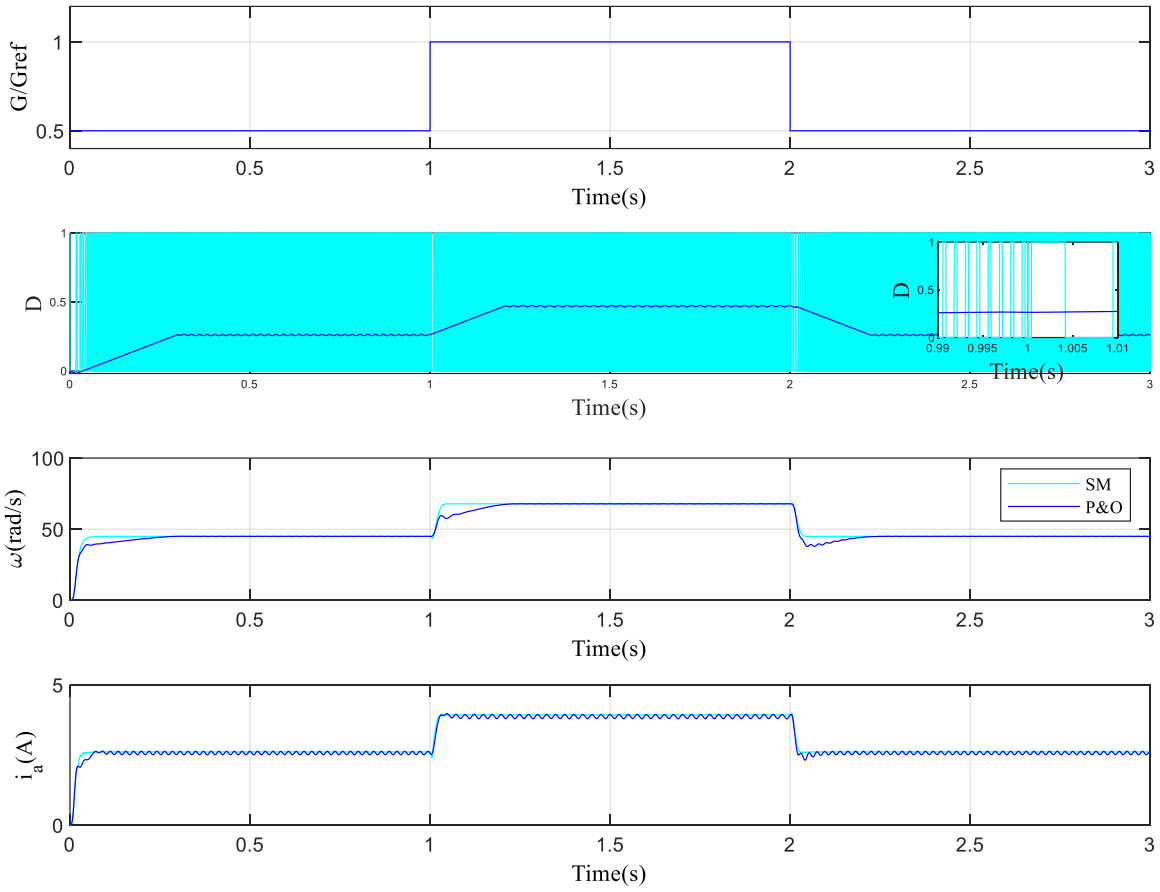


**Figure 7.** Irradiation (G/G$_{ref}$), duty cycle (D), speed ($\omega$), and armature current ($i_a$).

Figure 8 displays critical performance metrics, including the PV current ($I_p$), PV voltage ($V_p$), boost converter output voltage ($V_c$), and load torque ($T_L$). This figure serves to demonstrate the operational characteristics of the photovoltaic system under different load conditions, highlighting the efficiency of energy conversion throughout the system. The relationships among these parameters are vital for understanding the effectiveness of SMC in maintaining optimal performance.

Figure 9 showcases the achieved power output from the PV system, including a zoomed-in view that captures the abrupt changes experienced during operation. This detailed depiction provides insight into the transient response of SMC, illustrating how effectively the algorithm maintains power output during sudden fluctuations in irradiance. The figure reinforces the importance of SMC in providing stability and performance consistency in variable conditions.

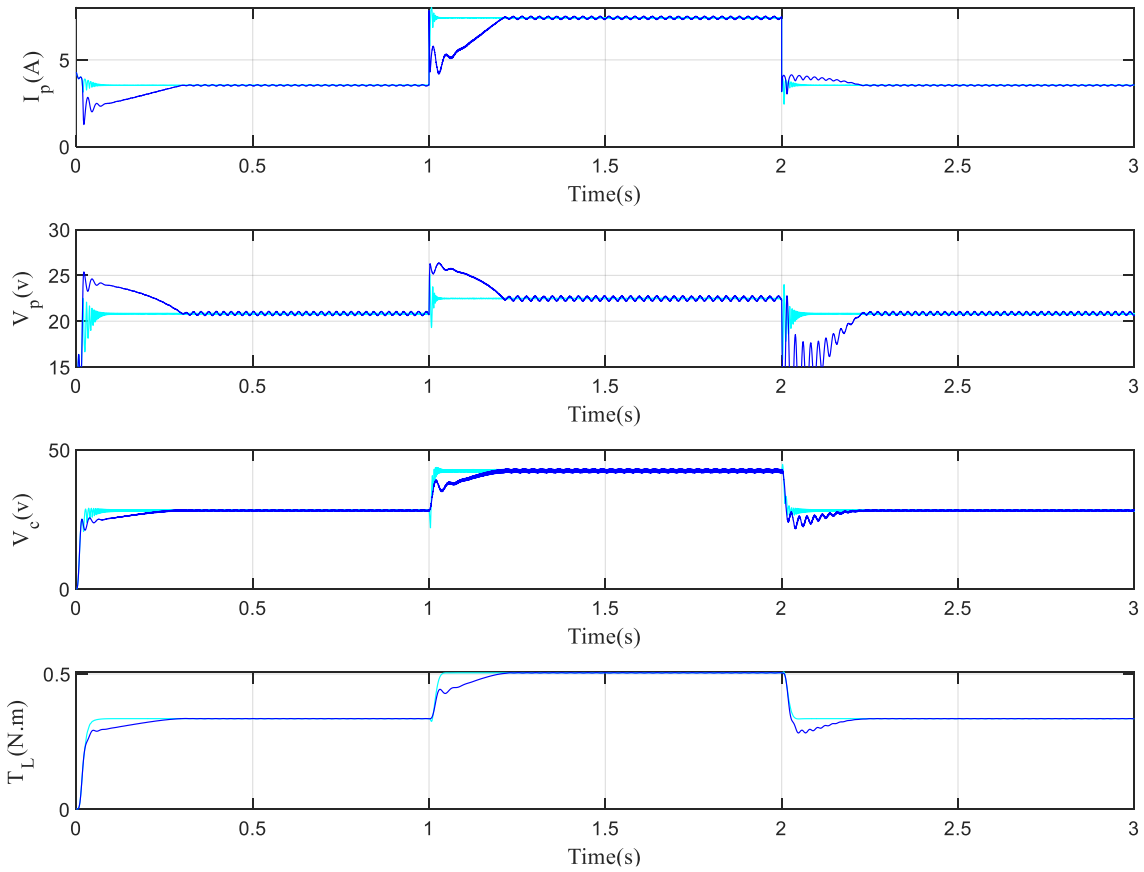


**Figure 8.** PV current ($I_p$), PV voltage ($V_p$), boost converter output voltage ($V_c$), load torque ($T_L$).

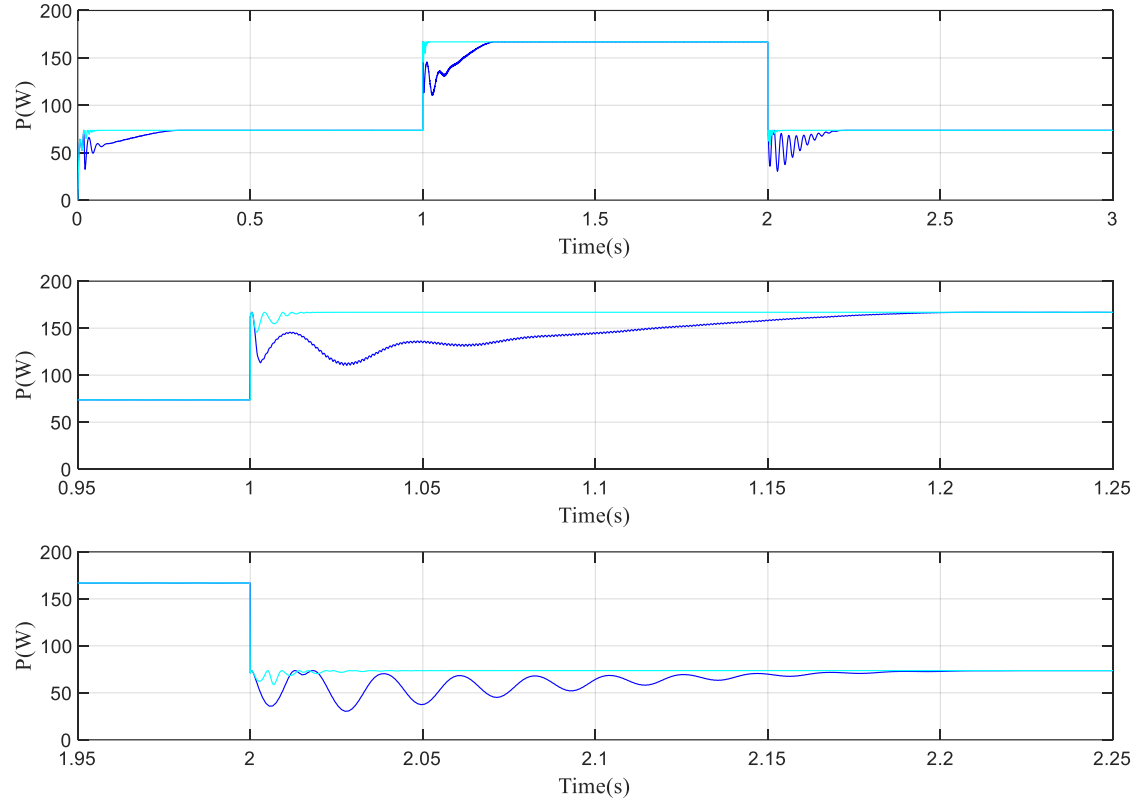


**Figure 9.** PV power (P).

Figure 10 compares the performance of the proposed PV pumping system under three distinct scenarios: without MPPT, using the Perturb and Observe (P&O) algorithm, and employing the Sliding Mode Control (SMC) algorithm. The data indicate that the flow rates achieved with SMC can be up to 70% higher than those obtained without any MPPT controller. This substantial enhancement underscores the effectiveness of SMC in maximizing the output power of the Photovoltaic Generator (PVG) and significantly improving water pumping performance. Moreover, the figure highlights the superior rapidity of response and reduced oscillations exhibited by SMC compared with traditional methods, further validating its applicability in PV-WPSs.

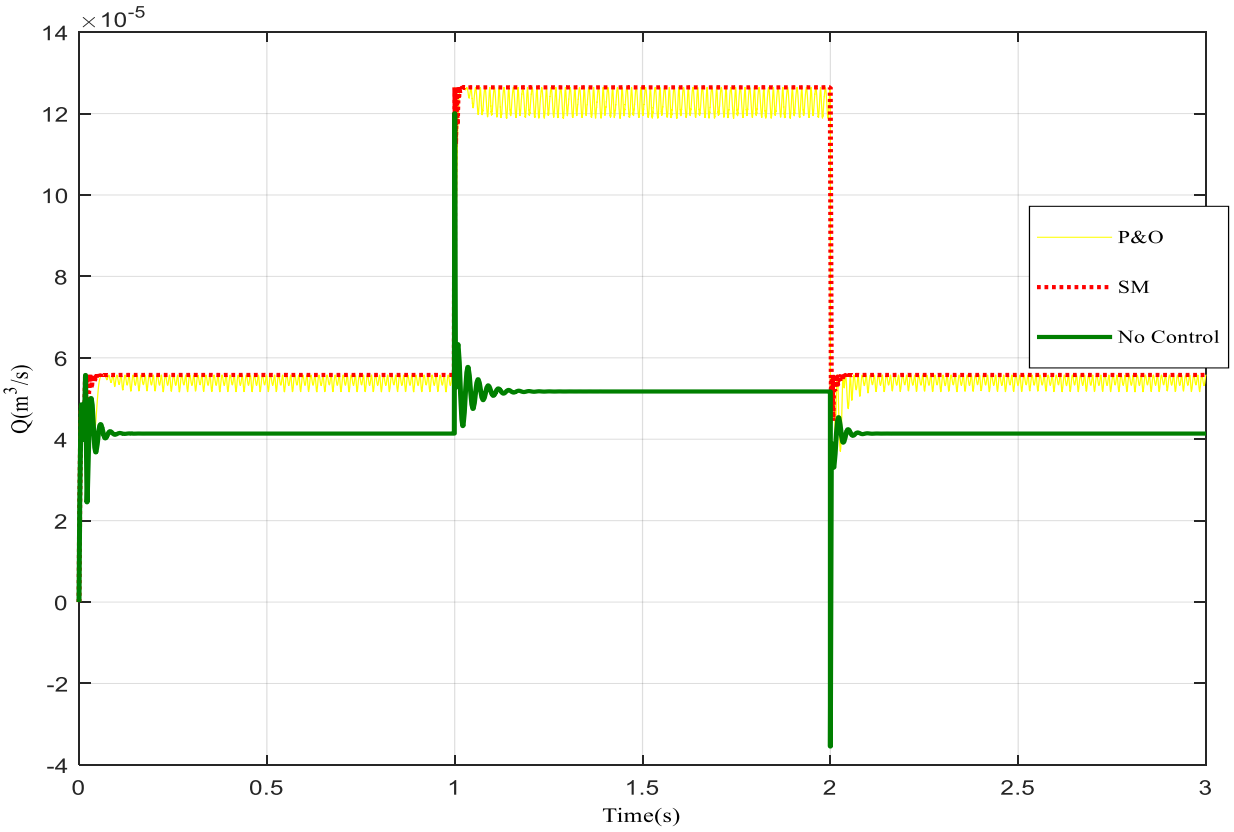


**Figure 10.** Water flow (Q).

In conclusion, unlike traditional methods, which may struggle to adapt to changing environmental conditions, SMC offers robust and dynamic control capabilities. By continuously adjusting the system parameters based on real-time feedback, SMC ensures precise tracking of the MPP of the PV panel, even under varying irradiation levels and load conditions. The adaptive characteristics of SMC allow it to harness the maximum power available from the PVG, thereby optimizing water flow rates.

### *4.2. Exprimental Result*

This section examines the overall control of the PV system. Figure 11 illustrates the hardware block diagram of the photovoltaic (PV) system, showcasing the interconnection between various components, including the PV panel, DC converter, and the controller, all interfaced through a PC. The PV system has undergone extensive experimental testing, and some of the results are presented in this section. A comparison study has been performed between the PV system using the standard P&O algorithm and the proposed MPPT SM controller to assess the effectiveness of the proposed control scheme. Often called Real-Time Computing (RTC), real-time control involves controlling the behavior of both software and hardware systems in real time.

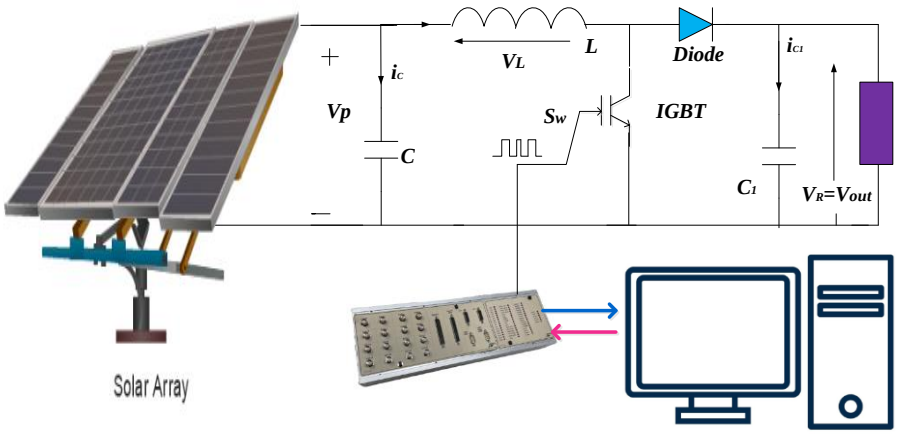


**Figure 11.** The hardware block diagram.

Digital Signal Processors (DSPs) are specialized microprocessors extensively used in power electronics for DC/DC converter and Pulse-Width Modulation (PWM) control. Known for their optimized architecture, DSPs are crucial in diverse fields such as medical devices, control systems, multimedia, military, telecommunications, automotive, and household appliances. Their high execution speed and specialized functions provide significant computing power and efficiency [65–67].

The DS1104 (DSP) controller has been chosen as the control platform, facilitating communication between the system's physical hardware and SIMULINK (MatlabR2021a). This integration is achieved by incorporating dSP input/output interface blocks into SIMULINK models. The effectiveness of the proposed control scheme is assessed by converting SIMULINK models to C-code using the Real-Time Workshop toolbox in SIMULINK/Matlab [66,67].

Through the use of the DSP graphical user interface (GUI), real-time supervision and monitoring of the system's behavior and performance are available. Users can observe and record live performance data and make real-time adjustments to the system parameters. The dSPACE DS1104 real-time control layout card is utilized in this study to implement the MPPT.

As depicted in Figure 11, the hardware setup is illustrated, while Figure 12 showcases the MPPT PV system hardware. The ATERSA A55 panels are feeding the boost converter and the load. Four ATERSA A55 PV panels have been installed in parallel on the roof for this study. All components utilized in this research are depicted in Figure 12, with:

Number 1 is the PV panels;
Number 2 is the Sensors outputs;
Number 3 is the Manually variable resistor;
Number 4 is the dSPACE card;
Number 5 is the Computer;
Number 6 is the DSP graphical user interface;
Number 7 is the DC boost converter.

On a PC, a digital signal processor card and the dSPACE DS1104 software (Control Desk Next Generation version 4.2.1) were used to acquire data and control the system. Sensors mounted in the boost converter provided the acquired measurements. Boost converter sensors provided measurements directly.

The output of the SMC controller (which is a digital signal) was sent to the DC/DC converter through a digital output of the dSPACE [12]. In this case, the switching frequency depended on the selected sample time because SMC output (0 or 1) would change in each sample time. In this work, all subsequent results were obtained at noon in Vitoria Gasteiz, Spain.


(**a**)

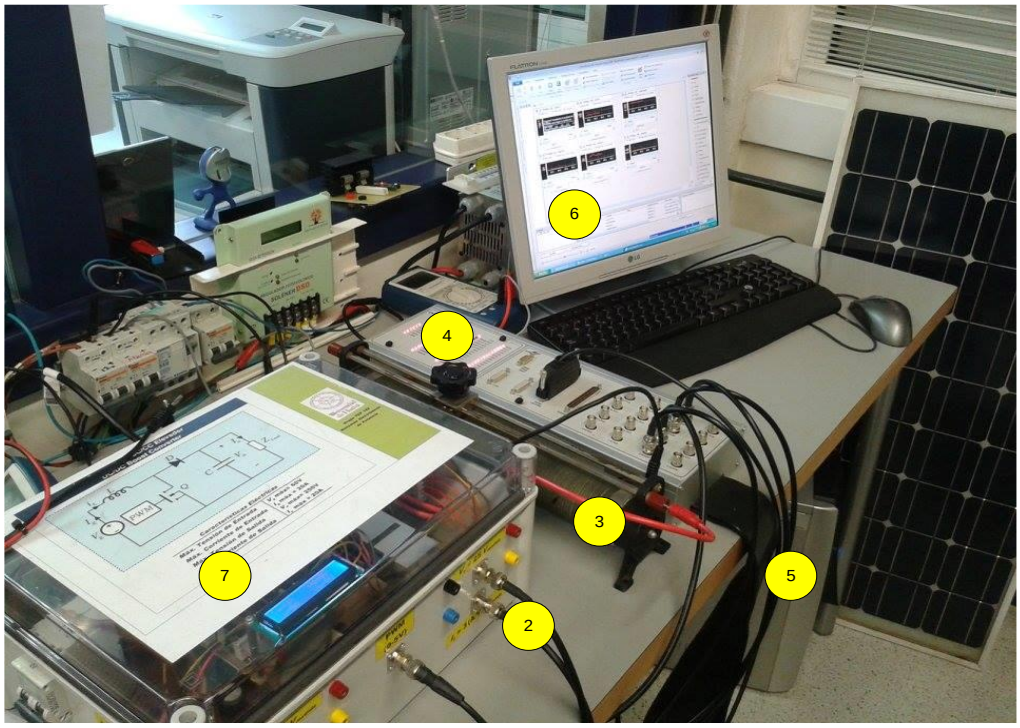


(**b**)

**Figure 12.** The system hardware: (**a**) $P_v$ panel and (**b**) DAC, boost converter, load, and computer.

A robustness test of the Sliding Mode (SM) system incorporating photovoltaic installation was conducted with a variation of the load, and the incident irradiation was defined as internal and external perturbation. After 20 s, the load value was manually modified to demonstrate the robustness of the SM controllers and their ability to maintain maximum power extraction. Despite the sudden variation in load, the system had undergone an abrupt internal perturbation (the load variation); at 20 s, it went from 14.1213 ohm to 27.5708 ohm. This variation represented a sudden change in the Water Pumping Systems (WPSs) connected to the PV panel. Moreover, the irradiation also presented a great variation from 580 to 220 W/m$^2$.

Figure 13 illustrates the evolution of voltage and current values at load terminals ($V_{out}$) and ($I_{out}$). It also illustrates the irradiation, power (P), current ($I_p$), and panel voltage ($V_p$).

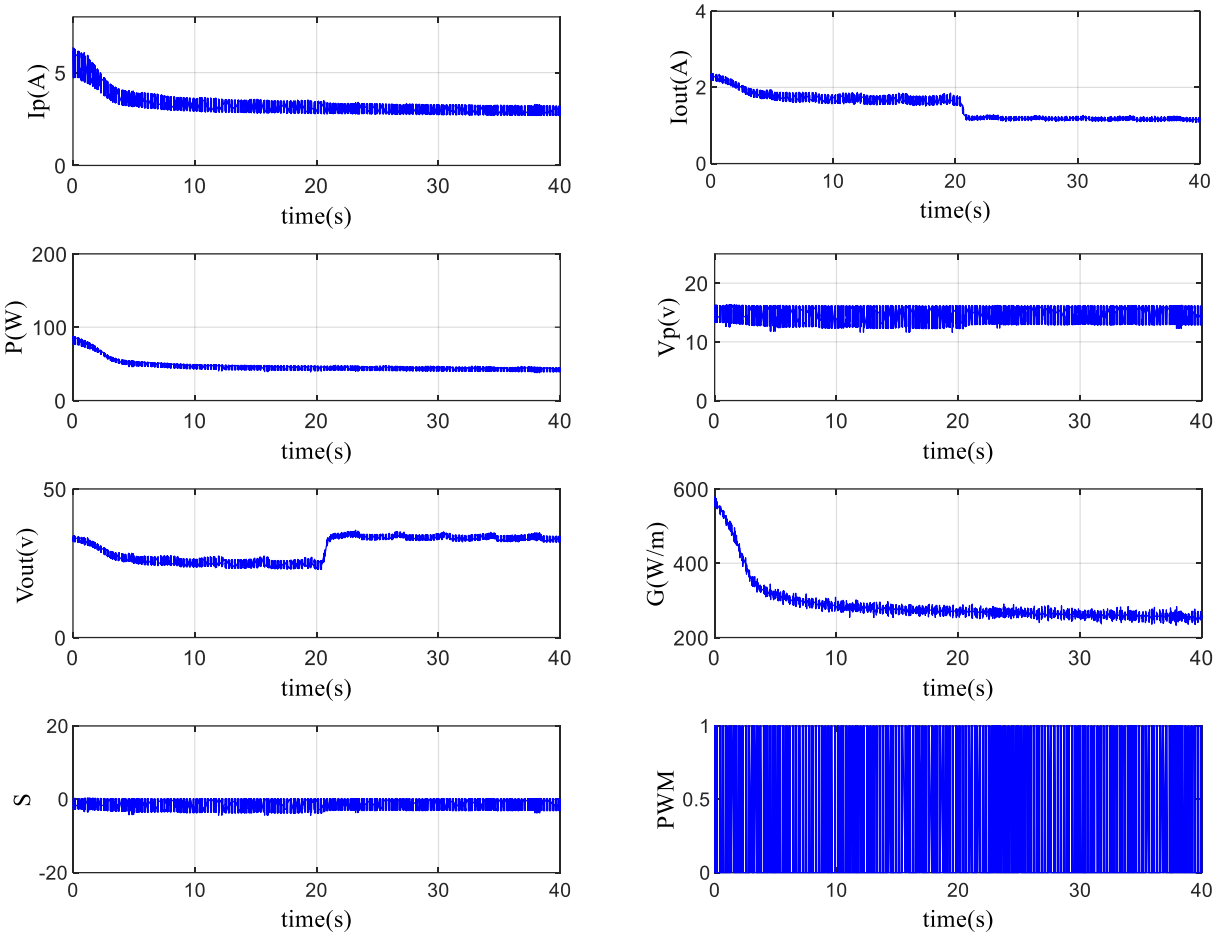


**Figure 13.** Evolution of system signals under variable irradiation and load with SMC.

Figure 14 depicts the experimental Power versus Voltage (P-V) and Current versus Voltage (I-V) characteristics for the ATERSA under different irradiation and temperature conditions. A load variation ranging from 0.1 Ω to 47.5 Ω was conducted to ascertain the panel's real characteristics, as shown in Figure 14. The red color indicates the obtained values of P-V and I-V during the application of SMC to the PV panel characteristics shown in Figure 13. These results underscore the efficacy of SMC in tracking the Maximum Power Point (MMP). As it is depicted in Figure 13, the irradiation (G) decreased dramatically by 80%. Despite significant variations in irradiation and load, the MPPT SM controller consistently operated within the MPPT zone where the ($V_p$), ($I_p$), and the power (P) were following the irradiation (G) variation. The results obtained by the SM controller demonstrated its robust design and effective tracking of maximum power. The SM controller also exhibited high sensitivity to sudden and rapid changes in irradiation, as illustrated in Figure 13. Despite internal changes where the load varied, the system consistently operated within the MPPT zone, as illustrated in Figure 14. This demonstrates the robustness of our control methodology in adapting to fluctuations and maintaining optimal performance even under dynamic load conditions. The effectiveness of our approach in sustaining MPPT operation amidst varying load characteristics highlights its potential for real-world applications where operational conditions may vary unpredictably.

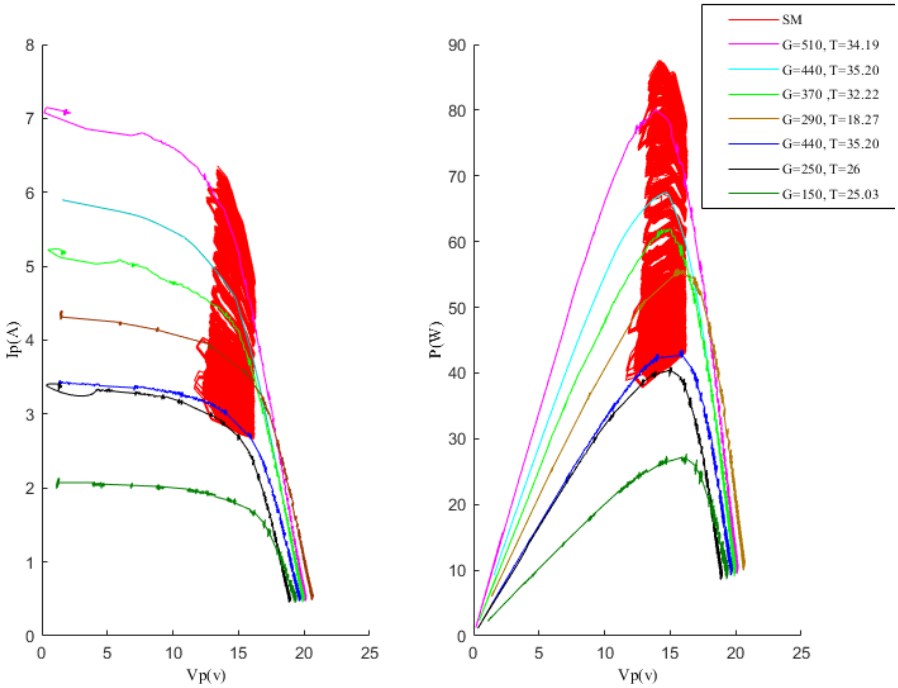


**Figure 14.** P-V and I-V characteristics and tracking path using SMC.

## 5. Conclusions

This paper presents a new method for optimizing Photovoltaic Water Pumping Systems (PV-WPSs) by introducing the Sliding Mode Control (SMC) technique and comparing its performance with the conventional Perturb and Observe (P&O) algorithms for Maximum Power Point Tracking (MPPT). The stability of the proposed SMC method was validated using Lyapunov's theory, demonstrating its robustness against internal and external disturbances.

Through simulation-based comparisons and real-time experiments, the efficiency of the SMC-based system was highlighted. The SMC controller successfully achieved MPPT under varying irradiation levels and load conditions, showing superior performance over traditional P&O algorithms. The results revealed that the SMC system could enhance water flow rates by up to 70% compared with systems without MPPT controllers.

Moreover, the experimental results confirmed the SMC controller's ability to maintain MPPT operation even under significant variations in irradiation and load fluctuations, ensuring efficient power extraction from the PV panel. The controller's high sensitivity to sudden environmental changes underscores its potential for reliable and efficient system performance.

Moving forward, the research will focus on developing a prototype based on the optimized SMC strategy to validate its practical effectiveness in real-world conditions. The prototype will be tested in environments representative of remote and off-grid locations to optimize water supply solutions sustainably. Upon successful testing and refinement, there are plans to advance the system towards commercialization, offering a scalable solution for sustainable water pumping and irrigation applications, particularly in reclaimed land developments and other areas with limited access to the electrical grid.

In conclusion, integrating SMC into PV-WPSs offers robust and dynamic control capabilities, significantly enhancing system performance and water flow rates. This advancement contributes not only to sustainable water supply solutions but also to the broader development of climate-resilient infrastructure in urban and rural settings.

**Author Contributions:** Conceptualization, M.F. and O.B.; methodology, M.F.; software, M.F.; validation, M.F. and O.B.; formal analysis, M.F.; investigation, M.F.; resources, M.F.; data curation, M.F.; writing—original draft preparation, M.F.; writing—review and editing, M.F. and O.B.; visualization, M.F.; supervision, O.B.; project administration, M.F.; funding acquisition, O.B. All authors have read and agreed to the published version of the manuscript.

**Funding:** The authors wish to express their gratitude to the Basque Government, through the project EKOHEGAZ II (ELKARTEK KK-2023/00051), to the Diputación Foral de Álava (DFA), through the project CONAVANTER, to the UPV/EHU, through the project GIU23/002, and to the Mobility Lab Foundation (CONV23/14) for supporting this work.

**Data Availability Statement:** The data supporting the findings of this study are available upon request from the corresponding author. Access to the data is subject to approval from the University of the Basque Country (UPV/EHU) in accordance with institutional policies.

**Conflicts of Interest:** The authors declare no conflict of interest.

## Nomenclature

| | |
|---|---|
| *G* | *Gref* Global, Reference insulation (W/m$^2$) |
| *I* | Light-generated current source (A) |
| *Ip*, *Vp* | Cell output current and voltage of the panel |
| *Rp*, *Rs* | Cell parallel and series resistance (Ω) |
| n, *Eg* | Solar ideal factor, Band gap energy (*ev*) |
| *Irs* | Reverse diode saturation current (A) |
| *KSCT* | Short circuit current temperature (A/°K) |
| *Tc*, *Tc_ref* | Cell junction, Reference temperature (°C) |
| *Iph* | Photon current (*A*) |
| *Ic* | Cell current (*A*) |
| *Vc* | Cell voltage (*V*) |
| *Id* | Diode current (*A*) |
| *Ish* | Shunt current (*A*) |
| *q* | Charge (Coulomb) |
| *α* | Ideality factor, A number between 1 and 2 |
| *β* | Boltzmann constant ($1.38 \times 10^{-23}$) |
| *T* | Absolute temperature (K) |
| *D* | Duty cycle |
| *Ns*, *Np* | Number of series, Parallel modules |
| ns | Number of series cells |
| Ra | Armature resistance (Ω) |
| La | Armature inductance |
| Ua | armature voltage (V) |
| f | constant viscous friction coefficient |
| J | the inertia Moment |
| Tem, TL | motor, load (pump) torque |
| Kt | back emf constant (also motor torque constant) |

## References

1. Sezen, S. Utilization of project support for renewable energy financing in public buildings: A solar carport feasibility example. *Int. J. Energy Stud.* **2024**, *9*, 347–367. [CrossRef]
2. Baig, H.; Sellami, N.; Chemisana, D.; Rosell, J.; Mallick, T.K. Performance analysis of a dielectric based 3D building integrated concentrating photovoltaic system. *Sol. Energy* **2014**, *103*, 525–540. [CrossRef]
3. Ibraheem, Y.; Piroozfar, P.; Farr, E.R.; Ravenscroft, N. Energy Production Analysis of Photovoltaic Shading Devices (PVSD) in Integrated Façade Systems (IFS). *Front. Built Environ.* **2020**, *6*, 81. [CrossRef]
4. Kabalci, Y.; Kabalci, E.; Canbaz, R.; Calpbinici, A. Design and implementation of a solar plant and irrigation system with remote monitoring and remote control infrastructures. *Sol. Energy* **2016**, *139*, 506–517. [CrossRef]
5. Garcia, L.; Chen, Y. Economic Feasibility of Solar-Powered Water Pumps with Tracking Systems. *J. Sustain. Agric.* **2023**.
6. Rao, D.N.M.; Sireesha, N.V.; Arjun, G.; Sami, M.A.; Gangadhar, S.R.; Vihal, T.; Kumar, D.G. Solar Tracking for Automation of Irrigation System. In *IOP Conference Series: Earth and Environmental Science*; IOP Publishing: Bristol, UK, 2024; Volume 1285.

7. Thompson, R.; El-Sayed, A. Integrating Solar Trackers with Smart Water Management Systems. *J. Environ. Manag.* **2024**.
8. Smith, J.; Johnson, R. Performance Analysis of Solar Tracking Systems for Water Pumping Applications. *Renew. Energy* **2022**.
9. Chandel, S.S.; Naik, M.N.; Chandel, R. Review of solar photovoltaic water pumping system technology for irrigation and com-munity drinking water supplies. *Renew. Sustain. Energy Rev.* **2015**, *49*, 1084–1099. [CrossRef]
10. Derbeli, M.; Barambones, O.; Silaa, M.Y.; Napole, C. Real-Time Implementation of a New MPPT Control Method for a DC-DC Boost Converter Used in a PEM Fuel Cell Power System. *Actuators* **2020**, *9*, 105. [CrossRef]
11. Katche, M.L.; Makokha, A.B.; Zachary, S.O.; Adaramola, M.S. A Comprehensive Review of Maximum Power Point Tracking (MPPT) Techniques Used in Solar PV Systems. *Energies* **2023**, *16*, 2206. [CrossRef]
12. Farhat, M.; Barambones, O.; Sbita, L. Efficiency optimization of a DSP-based standalone PV system using a stable single input fuzzy logic controller. *Renew. Sustain. Energy Rev.* **2015**, *49*, 907–920. [CrossRef]
13. Melzein, I.; Kurdi, M.; et Harrye, Y. Optimizing the Maximum Power of Photovoltaic System Using Modified Incre-mental Conductance Algorithm Operating Under Varying Dynamic Climatic Conditions. *Int. J. Comput. Digit. Syst.* **2024**, *15*, 1–20. [CrossRef] [PubMed]
14. Fapi, C.B.N.; Wira, P.; Kamta, M.; Tchakounté, H.; Colicchio, B. Simulation and dSPACE hardware implementation of an improved fractional short-circuit current MPPT algorithm for photovoltaic system. *Appl. Sol. Energy* **2021**, *57*, 93–106. [CrossRef]
15. Charaabi, A.; Zaidi, A.; Barambones, O.; Zanzouri, N. Implementation of adjustable variable step based backstepping control for the PV power plant. *Int. J. Electr. Power Energy Syst.* **2022**, *136*, 107682. [CrossRef]
16. Khalaf, H.M.; Mohammed, J.A.K.; Altahir, A.A.R. *Simulation of Pneumatic Actuators under Fuzzy Logic Control for Driving Solar Tracking System*; Transdisciplinary Research and Education Center for Green Technologies, Kyushu University: Fukuoka, Japan, 2024; pp. 1848–1855.
17. Sotoudeh-Anvari, A. A critical review on theoretical drawbacks and mathematical incorrect assumptions in fuzzy OR methods: Review from 2010 to 2020. *Appl. Soft Comput.* **2020**, *93*, 106354. [CrossRef]
18. Kushnir, A.; Kopchak, B.; Oksentyuk, V. Development of heat detector based on fuzzy logic using arduino board microcontroller. In Proceedings of the 2023 17th International Conference on the Experience of Designing and Application of CAD Systems (CADSM), Jaroslaw, Poland, 22–25 February 2023; IEEE: Piscataway, NJ, USA, 2023; pp. 1–5. [CrossRef]
19. Farhat, M.; Flah, A.; Sbita, L. Photovoltaic maximum power point tracking based on ANN control. *Int. Rev. Model. Simul.* **2014**, *7*, 474–480. [CrossRef]
20. Das, S.; Goswami, R.S. Review, Limitations, and future prospects of neural network approaches for brain tumor classification. *Multimed. Tools Appl.* **2024**, *83*, 45799–45841. [CrossRef]
21. Selma, B.; Bounadja, E.; Belmadani, B.; Selma, B. Improved performance and robustness of synchronous reluctance machine control using an advanced sliding mode and direct vector control. *Adv. Control. Appl. Eng. Ind. Syst.* **2024**, *6*, e178. [CrossRef]
22. Djouadi, H.; Ouari, K.; Belkhier, Y.; Lehouche, H. Real-Time HIL Simulation of Nonlinear Generalized Model Predictive-Based High-Order SMC for Permanent Magnet Synchronous Machine Drive. *Int. Trans. Electr. Energy Syst.* **2024**, *2024*, 5536555. [CrossRef]
23. Elbaksawi, O. Design of photovoltaic system using buck-boost converter based on MPPT with PID controller. *Univers. J. Electr. Electron. Eng.* **2019**, *6*, 314–322. [CrossRef]
24. Yu, L.; Huang, J.; Luo, W.; Chang, S.; Sun, H.; Tian, H. Sliding-mode control for PMLSM position control—A review. *Actuators* **2023**, *12*, 31. [CrossRef]
25. Charishma, M.; Chandrasekhar, J.N. Comparison of PI, Fuzzy and Sliding Mode Control Techniques in Speed Control of BLDC Motor. *Int. J. Eng. Res. Technol.* **2019**, *8*, 29–35. [CrossRef]
26. Zhou, J.; Zhou, J.; Yang, H.; Huang, L. Passive Super-Twisting Second-Order Sliding Mode Control Strategy for Input Stage of MMC-PET. *Energies* **2024**, *17*, 2036. [CrossRef]
27. Kanouni, B.; Badoud, A.E.; Mekhilef, S.; Bajaj, M.; Zaitsev, I. Advanced efficient energy management strategy based on state machine control for multi-sources PV-PEMFC-batteries system. *Sci. Rep.* **2024**, *14*, 7996. [CrossRef] [PubMed]
28. Betka, A.; Moussi, A. Performance optimization of a photovoltaic induction motor pumping system. *Renew. Energy* **2004**, *29*, 2167–2181. [CrossRef]
29. Akbaba, M. Matching Induction Motors to PVG for Maximum Power Transfer. *Desalination* **2007**, *209*, 31–38. [CrossRef]
30. Senjyu, T.; Veerachary, M.; Uezato, K. Steady-state analysis of PV supplied separately excited DC motor fed from IDB converter. *Sol. Energy Mater. Sol. Cells* **2002**, *71*, 493–510. [CrossRef]
31. Guerrero-Ramirez, E.; Martinez-Barbosa, A.; Contreras-Ordaz, M.A.; Guerrero-Ramirez, G.; Guzman-Ramirez, E.; Barahona-Avalos, J.L.; Adam-Medina, M. DC Motor Drive Powered by Solar Photovoltaic Energy: An FPGA-Based Active Disturbance Rejection Control Approach. *Energies* **2022**, *15*, 6595. [CrossRef]
32. Khalid, H.M.; Rafique, Z.; Muyeen, S.M.; Raqeeb, A.; Said, Z.; Saidur, R.; Sopian, K. Dust accumulation and aggregation on PV panels: An integrated survey on impacts, mathematical models, cleaning mechanisms, and possible sustainable solution. *Sol. Energy* **2023**, *251*, 261–285. [CrossRef]
33. Gholami, A.; Ameri, M.; Zandi, M. Step-by-step guide to model photovoltaic panels: An Up-To-Date comparative review study. *IEEE J. Photovolt.* **2022**, *12*, 915–928. [CrossRef]
34. Vaghela, M.A.; Mulla, M.A. Small-signal model of two-phase interleaved coupled inductor-based high step-up gain converter in DCM. *Electr. Eng.* **2023**, *105*, 1565–1583. [CrossRef]

35. Guo, Q.; Bahri, I.; Diallo, D.; Berthelot, E. Model predictive control and linear control of DC–DC boost converter in low voltage DC microgrid:An experimental comparative study. *Control. Eng. Pract.* **2023**, *131*, 105387. [CrossRef]
36. Farhat, M.; Barambones, O.; Sbita, L. A new maximum power point method based on a sliding mode approach for solar energy harvesting. *Appl. Energy* **2017**, *185*, 1185–1198. [CrossRef]
37. Shrestha, R.; Dhakal, A.R.; Thakur, S.; Subedi, D.; Sharma, M. Design of Digital Solar Water Pump Using Microcontroller ATmega 32. *Electr. Sci. Eng.* **2022**, *4*, 11–24. [CrossRef]
38. Sharmila, B.; Srinivasan, K.; Devasena, D. Modelling and performance analysis of electric vehicle. *Int. J. Ambient Energy* **2022**, *43*, 5034–5040. [CrossRef]
39. Yang, X.; Deng, W.; Yao, J. Neural network based output feedback control for DC motors with asymptotic stability. *Mech. Syst. Signal Process.* **2022**, *164*, 108288. [CrossRef]
40. Mohammedi, A.; Rekioua, D.; Mezzai, N. Experimental Study of a PV Water Pumping System. *J. Electr. Syst.* **2013**, *9*, 212–222.
41. Barbhuiya, I.; Singha, P.; Singh, S.K. Positive displacement pumps. In *Transporting Operations of Food Materials within Food Factories*; Elsevier: Amsterdam, The Netherlands, 2022.
42. Hossain, M.I.; Rahman, M.A. Performance Analysis of MPPT Techniques for PV Systems: A Review. *Renew. Sustain. Energy Rev.* **2021**, *135*, 110167.
43. Khan, M.J.; Kumar, S. Comparative Study of Maximum Power Point Tracking Techniques for Photovoltaic Systems. *Energy Rep.* **2020**, *6*, 123–130.
44. Moussa, A.; Zidan, H. A Comparative Study of Fuzzy Logic and ANN Based MPPT Controllers for PV Systems. *J. Sol. Energy Eng.* **2019**, *141*, 041002.
45. Chen, L.; Wang, H. Fuzzy fractional control for robotic systems: A review. *Robot. Auton. Syst.* **2022**, *146*, 103843.
46. Zhang, Y.; Liu, H. Cost-effective fuzzy control strategies for automated manufacturing systems. *IEEE Trans. Autom. Sci. Eng.* **2021**, *18*, 1450–1460.
47. Anbalagan, P.; Joo, Y.H. Design of memory-based adaptive integral sliding-mode controller for fractional-order T-S fuzzy systems and its applications. *J. Frankl. Inst.* **2020**, *357*, 3672–3691. [CrossRef]
48. Yuan, J.; Shi, B.; Wang, Y. Control and synchronization of fractional unified chaotic systems with a single sliding mode controller. In Proceedings of the 33rd Chinese Control Conference, Nanjing, China, 28–30 July 2014; IEEE: Piscataway, NJ, USA, 2014; pp. 1800–1805.
49. Machado, J.T. The effect of fractional order in variable structure control. *Comput. Math. Appl.* **2012**, *64*, 3340–3350.
50. Feng, Y.; Han, F.; Yu, X. Chattering free full-order sliding-mode control. *Automatica* **2014**, *50*, 1310–1314. [CrossRef]
51. Efe, M.Ö. Fractional order sliding mode control with reaching law approach. *Turk. J. Electr. Eng. Comput. Sci.* **2010**, *18*, 731–748. [CrossRef]
52. Laware, A.; Bhavsar, V.; Shinde, P.; Lokhande, R. Design of Sliding Mode Control Strategy for DC Motor. *Int. J. Sci. Technol. Eng.* **2023**, *11*, 7548–7552. [CrossRef]
53. Shiledar, S.R.; Malwatkar, G.M. Comparison of Discrete Time Sliding Manifold and Its Impact on System Dynamics. In *Smart Sensors Measurement and Instrumentation: Select Proceedings of CISCON 2021*; Lecture Notes in Electrical Engineering; Springer Nature: Singapore, 2023. [CrossRef]
54. Deffaf, B.; Hamoudi, F.; Debdouche, N.; Chebabhi, A. Comparative analysis between Backstepping, Sliding mode and PI control applied to Shunt Active Filter. In Proceedings of the 2022 2nd International Conference on Advanced Electrical Engineering (ICAEE), Constantine, Algeria, 29–31 October 2022; IEEE: Piscataway, NJ, USA, 2022; pp. 1–6. [CrossRef]
55. Sakri, D.; Laib, H.; Farhi, S.E.; Golea, N. Sliding mode approach for control and observation of a three phase AC-DC pulse-width modulation rectifier. *Electr. Eng. Electromech.* **2023**, *2*, 49–56. [CrossRef]
56. Ruderman, M.; Voss, B.; Fridman, L.; Reger, J. Disturbance sensitivity analysis and experimental evalu-ation of continuous sliding mode control. *arXiv* **2022**, arXiv:2208.06608. [CrossRef]
57. Haghighi, A.; Ziaratban, R. A non-integer sliding mode controller to stabilize fractional-order non-linear systems. *Adv. Differ. Equ.* **2020**, *2020*, 503. [CrossRef]
58. Mayssa, F.; Sbita, L. Advanced ANFIS-MPPT Control Algorithm for Sunshine Photovoltaic Pumping Systems. In Proceedings of the First International Conference on Renewable Energies and VEhicular Technology, Nabeul, Tunisia, 26–28 March 2012; pp. 167–172.
59. Chiliveri, V.R.; Kalpana, R.; Subramaniam, U.; Muhibbullah, M.; Padmavathi, L. Novel reaching law based predictive sliding mode control for lateral motion control of in-wheel motor drive electric vehicle with delay estimation. *IET Intell. Transp. Syst.* **2024**, *18*, 872–888. [CrossRef]
60. Ali, M.H.M.; Mohamed, M.M.S.; Ahmed, N.M.; Zahran, M.B.A. Comparison between P&O and SSO techniques based MPPT algorithm for photo-voltaic systems. *Int. J. Electr. Comput. Eng.* **2022**, *12*, 32–40. [CrossRef]
61. Ali, A.I.M.; Mohamed, H.R.A. Improved P&O MPPT algorithm with efficient open-circuit voltage estimation for two-stage grid-integrated PV system under realistic solar radiation. *Int. J. Electr. Power Energy Syst.* **2022**, *137*, 107805. [CrossRef]
62. Farhat, M.; Barambones, O.; Sbita, L. A Real-Time Implementation of Novel and Stable Variable Step Size MPPT. *Energies* **2020**, *13*, 4668. [CrossRef]
63. Chen, J.; Yau, H.; Hung, W. Design and Study on Sliding Mode Extremum Seeking Control of the Chaos Embedded Particle Swarm Optimization for Maximum Power Point Tracking in Wind Power Systems. *Energies* **2014**, *7*, 1706–1720. [CrossRef]

64. Razmjooei, H.; Shafiei, M.H.; Palli, G.; Arefi, M.M. Non-linear finite-time tracking control of uncertain robotic manipulators using time-varying disturbance observer-based sliding mode method. *J. Intell. Robot. Syst.* **2022**, *104*, 36. [CrossRef]
65. Huang, X.; Tang, R.; Zhou, Y. DSP-based parallel optimization for real-time video stitching. *J. Real-Time Image Process.* **2023**, *20*, 28. [CrossRef]
66. Villalón, A.; Muñoz, C.; Muñoz, J.; Rivera, M. Fixed-Switching-Frequency Modulated Model Predictive Control for Islanded AC Microgrid Applications. *Mathematics* **2023**, *11*, 672. [CrossRef]
67. Kwan, A.K.; Helaoui, M.; Boumaiza, S.; Smith, M.R.; Ghannouchi, F.M. Wireless communications transmitter performance enhancement using advanced signal processing algorithms running in a hybrid DSP/FPGA platform. *J. Signal Process. Syst.* **2009**, *56*, 187–198. [CrossRef]